Electronic Supplementary Material (ESI) for Lab on a Chip.

Supporting Information

Microflow sensing and control using an in-channel birefringent biomembrane

Nan Jia,[1] Tianyang Deng,[1] Charles Larouche,[2] Tigran Galstain,[3] André Bégin-Drolet,[2] Jesse Greener[1,4]*

[1] Département de Chimie, Faculté des sciences et de génie, Université Laval, Québec City, QC, Canada

[2] Département de génie mécanique, Faculté des sciences et de génie, Université Laval, Québec, QC G1V 0A6, Canada

[3] Centre d'optique, photonique et laser, Département de physique, génie physique et optique, Faculté des sciences et de génie, Université Laval, Québec, QC G1V 0A6, Canada

[4] CHU de Québec, centre de recherche du CHU de Québec, Université Laval, Québec, QC G1L 3L5, Canada

* Corresponding author: jesse.greener@chm.ulaval.ca

Sections

Section S1-Experiments cycling pH

We validated the sensitivity of the membrane to pH by dynamic experiments in which the liquid admitted to both sides of the chitosan membrane flow chamber were alternated between solutions with pH 13 and pH 7.4. Importantly, the equilibrium RB at each pH is measurably different, opening the door to pH sensing using the membrane. It should be noted that the flow rates of the pumps after startup were validated to be accurate within 2 μL min^{-1}. This difference is too insignificant to account for the differences observed in RB, therefore, we attribute these changes to the solution pH. We also observed a transient overshoot to low RB following switching from high to low pH before reaching an equilibrium RB. The cause for this decrease is not known, but is hypothesized to be related to flow disturbances related to switching pumps. Further studies are underway to validate this hypothesis.

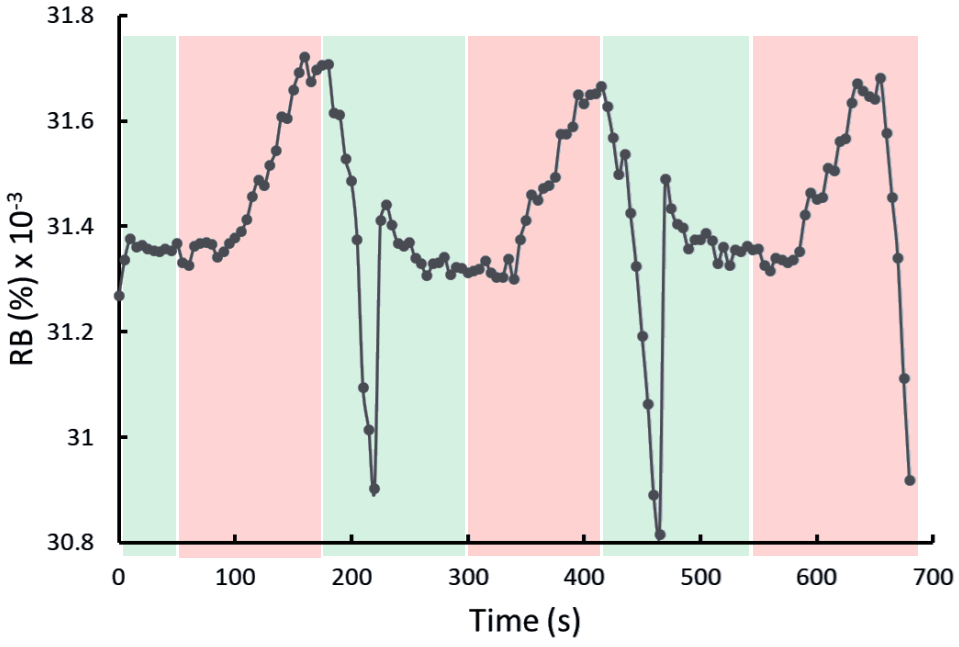

Figure S1. Chitosan RB response to oscillating pH solutions being admitted to the flow meter device. Green boxes indicate admission of 7.4 pH PBS buffer, and pink boxes admission of 13 pH solution. Flow rate was constant during the experiment (60 µL min^{-1}), though unintentional variations while switching pumps may have occurred.

Section S2-Bubbles and bacterial interference

To understand the effect of the interference effect from bubbles, we deliberately introduced them into the chitosan membrane sensor chamber. In the first experiment, the RB performed steadily until approximately 7 hours, when a bubble entered the chitosan membrane chamber and contacted the membrane. The bubble moved through the chamber over the next 8 hours before finally exiting. The resulting RB showed a complex change in intensity during that time, followed by a rapid decrease in intensity, which continued to decrease until it reached a plateau that was much less bright than before the bubble had arrived (Figure S2a). Indeed, the bubble was partially blocking the channel and could have had a complex influence on the fluid pressure, velocity and shear stress. This, in combination with the residual effects on RB even after the bubble had exited, indicates that bubbles have a strong and undesirable effect on the membrane performance.

Next, we considered the effect of presence of bacteria on membrane performance. The local flow rate within a microfluidic channel is often exploited in bacterial growth assays. For example, excessive shear stress caused by high flow rates can lead to physical damage, disruption of cell adhesion, and effects on the formation of biofilms, as our group has shown previously.[1-3] Unless volumetric flow systems are used, these and other applications can result in cellular chemiotaxis, which can cause interactions between the microorganisms and the flow rate meter, even if the flow rate meter is placed in an upstream of the bacterial samples.[4] After forming a membrane and obtaining a calibration curve, we cultured a biofilm (from the gut

bacteria of the insect *Zophobas morio)* beside the membrane but isolated the biofilm growth from the membrane with a co-flow of pure water that did not support bacterial growth. This was accomplished by flowing nutrient solution into inlet 3 and DI water at inlets 1, 2, and 4 (Figure S2b). Even though no biofilm could grow in the nutrient-depleted water stream against the membrane, high-resolution images show that individual bacteria accumulated against the membrane, likely due to unsuccessful foraging for new nutrient sources in the co-flowing water stream. The resulting RB is shown as a function of time in Figure S2b. In that figure a decrease in RB is observed after about 3 hours following inoculation of the biofilm-forming bacteria. The complex interactions between the biofilm and its ejected bacteria, together with the flow properties near the membrane and the membrane sensitivity, are difficult to decipher. For example, bacterial cells at the membrane surface could have potentially formed a barrier between the membrane and the liquid shear field, thus reducing the shear stresses applied to the membrane. In addition, the biofilm could change the flow fields around it, resulting in a faster flow field in the vicinity of the membrane. On the balance, these competing interferences served to reduce the membrane RB, which indicates that the presence of even a thin observed layer of bacteria appears to have a strong influence on the membrane performance. This influence could be related to extracellular polymeric materials excreted by the cells when they found the membrane surface. Although the interactions are too complex to evaluate here, the sum total

indicates that a sterile environment is crucial for good membrane performance.

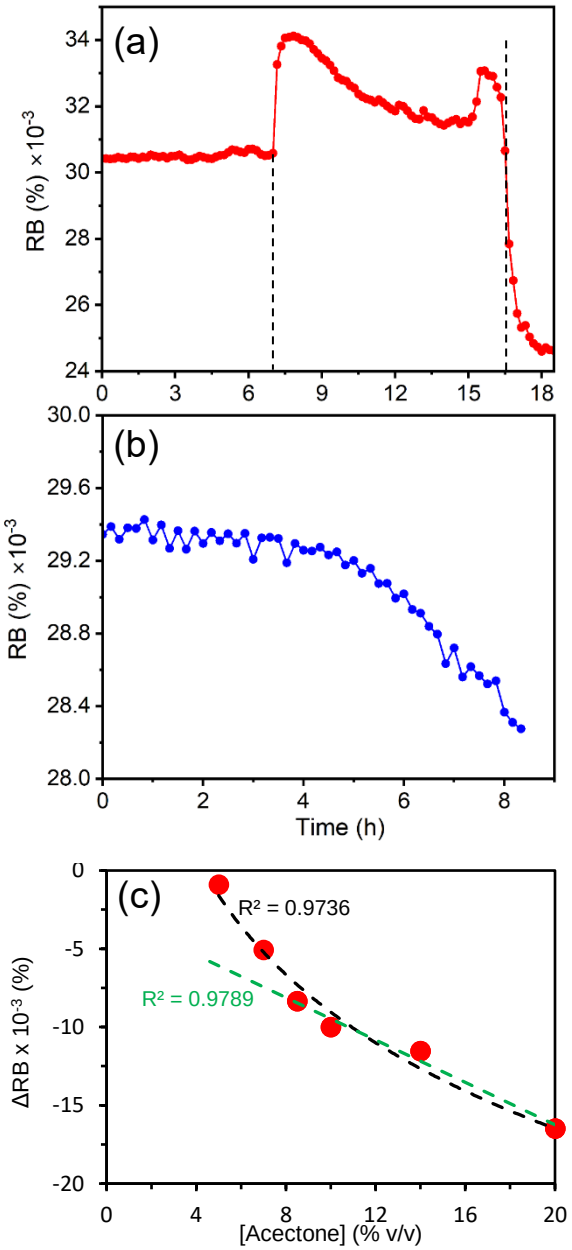

Figure S2. Changes in relative birefringence (a) during the transit of an air bubble through the membrane chamber (marked by dashed lines) and (b) following inoculation of biofilm-forming bacteria in the chitosan membrane chamber. The x-axis label applies to both (a) and (b). (c) Change in RB with increasing acetone concentration in a binary acetone/water mixture flowing at 60 μL min^{-1} (red data points). Two fittings are presented which attempt to capture trends either by evaluating the linear portion (above 8% acetone, green dashed line) or via a logarithmic-scale (black dashed line) accounting for the full-scale behaviour. The RB under pure aqueous conditions was approximately 30 × 10^{-3} %.

A third type of interference relates to the quality of the solution. To test this, we changed the concentration of the acetone component in a acetone/water binary mixture, while keeping the flow rate constant. Above 5 % (v/v) the acetone caused the membrane to dehydrate and become reduced in RB (Figure S2c). This trend continued progressively over the range of concentrations attempted (5-20%) and could be fit to a calibration curve. We note that two calibration curves fit the results with approximately the same fitting quality ($R^2 > 0.97$). These included a linear fit above 8% acetone and a logarithmic fit over the entire concentration range. It was observed that the membrane sensitivity improved and stabilized after several acetone exposure cycles. Therefore, in addition to obtaining a wider response curve, a pretreatment protocol should be developed.

Section S3-Flow control using a chitosan-based flow meter measurement in a closed-loop controller

Lastly, we developed an algorithm to undertake image analysis of the chitosan membrane as a measurement feedback to control the pump flow rate. The basis of operation includes the generation of a calibration curve and a control sequence wherein the RB brightness is compared to the calibration curve to obtain an updated pressure settings to for the pump.

The flowchart in Figure S3a shows how the calibration was performed. After initializing the required variables, the program runs an infinite loop during which the states of two interrupt buttons are continually read. When the first button is pressed, it allows the user to enter a desired pressure in a dialog box. The command is sent to the pressure pump. A delay of 5 seconds is introduced to allow the pressure to settle before measurements. Then, the algorithm takes a snapshot using camera's open-source libraries, processes the image to evaluate the brightness

of the membrane and reads the commercial flowmeter with Fluigent's open-source libraries. Those last steps are performed 3 times via a FOR loop. If the second button is not pressed, the user can add as many calibration data points as desired using the method discussed above. Otherwise, the WHILE loop breaks, and this leads to closed the program.

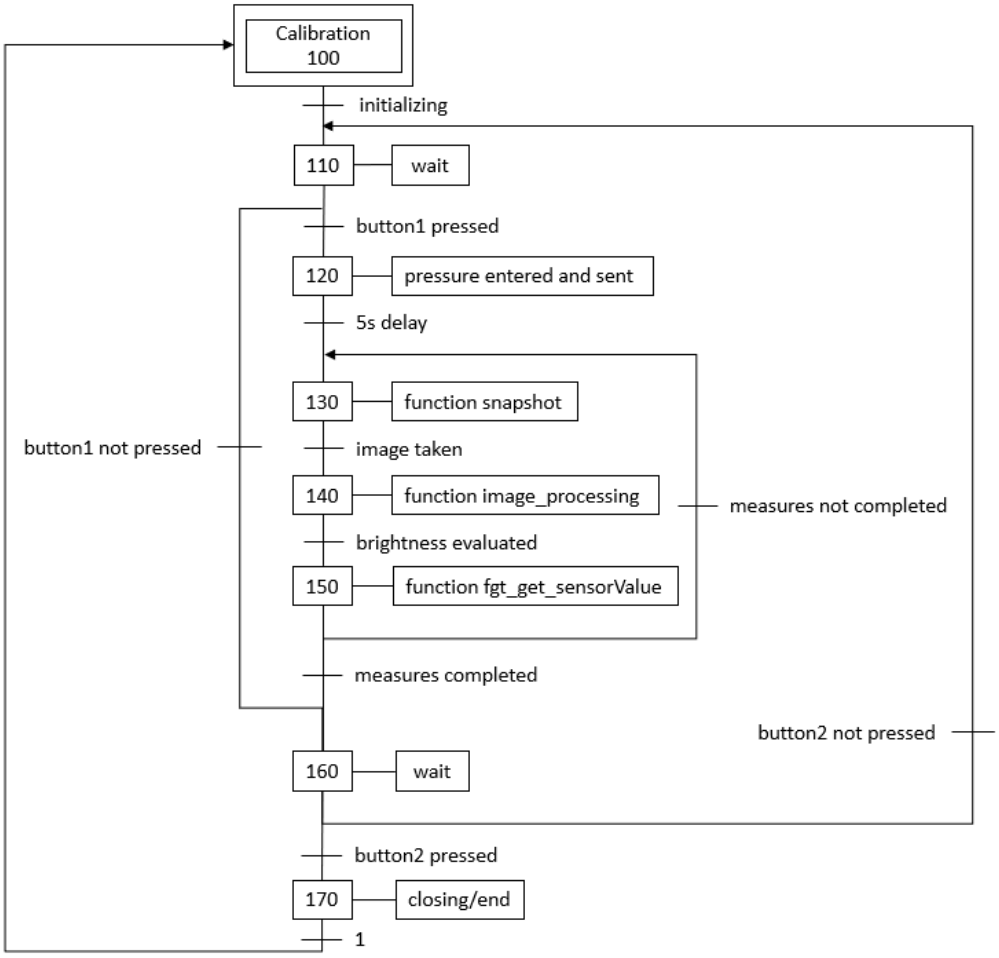

Figure S3a. Flow chart for the calibration algorithm.

Next, the control loop is run during a control sequence in an infinite loop (Figure S3b). During a cycle, the control algorithm calls 4 sub-functions. The first sub-function is called "snapshot", and it uses pre-existing functions from *Lumenera*'s open-source libraries that enable a connection between *MATLAB* and the Infinity 3 camera. The second sub-function processes the

captured image by applying a double integral on the recorded pixels array. The value obtained is the brightness index of the membrane. This leads to the next step, which is called “flowmeter”. It converts the RB to the corresponding flow rate using information gathered during the calibration. Finally, a pressure command is generated by a closed-loop PID controller based on the current measurement and the desire flow rate (set point). The WHILE loop can be broken with a push-button. In the closing steps, the camera and the pressure pump are correctly disconnected, and the results are plotted and recorded into an Excel file.

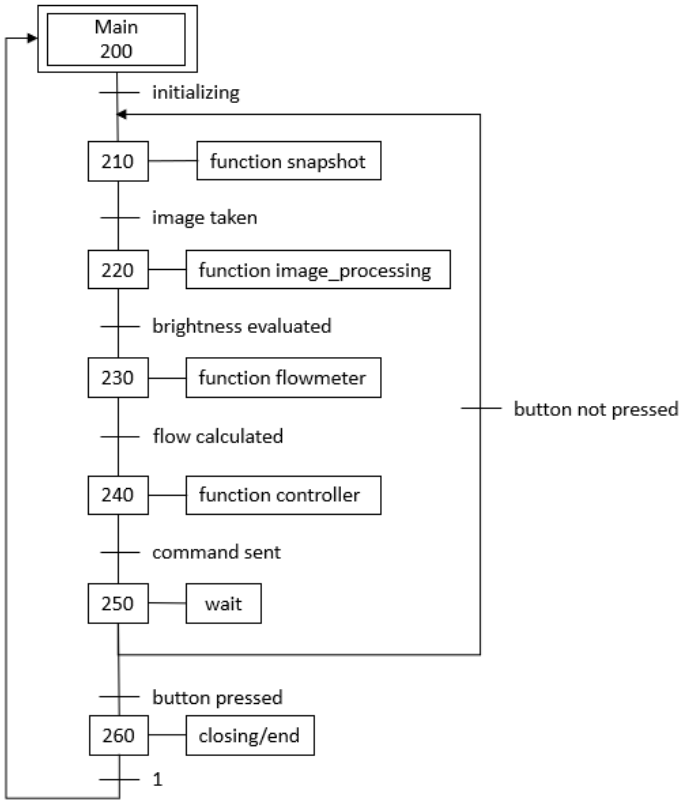

Figure S3b. Flow chart for the control algorithm.

The sub-function “controller” was developed using PID theory (Figure S3c). It first calculates the error between the current measured flow rate and the set point, and then the algorithm generates a pressure command to reach the desired flow rate. The proportional, integral and

derivative gains have been tuned immediately before the tests, because backpressure influences those parameters. Through the next step, the command becomes saturated to avoid sending the pump to a negative or too high pressure. At this stage, the command is ready to be sent to the pump. Finally, a preparatory calculation is performed for the next loop.

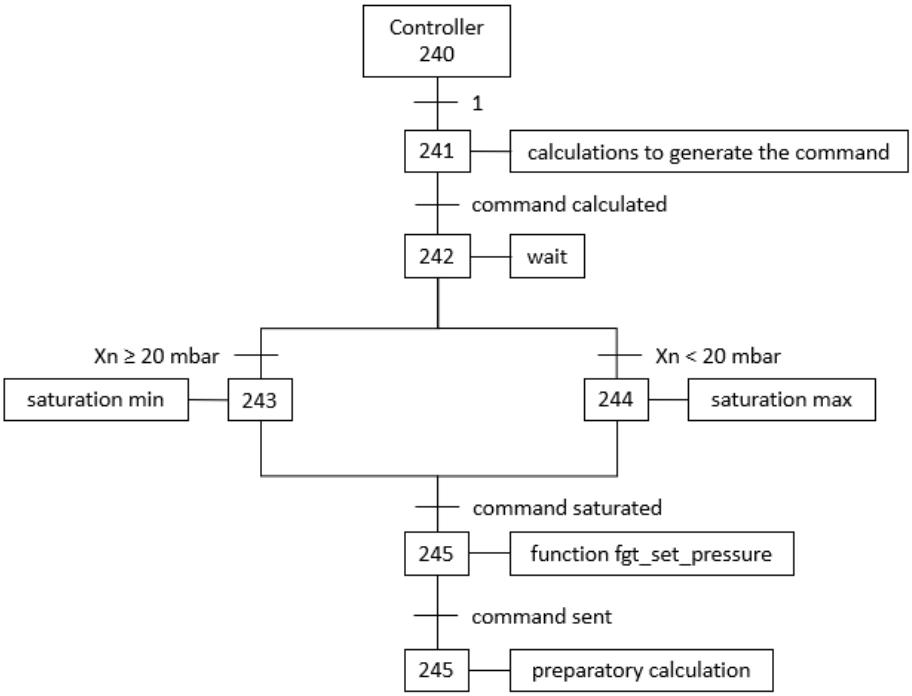

Figure S3c. Flow chart for the PID control loop (sub-function "controller")

Section S4-Reproducing an arbitrary flow profile

In the main paper we included results from an arbitrary wave function, rather than static set-points. The arbitrary waveform used was defined by the following function:

$$Q(t) = 2.6\times10^{-3}t^3\text{-}30.0t^2 + 8.1t + 2.2 \qquad \text{(Eqn. S1)}$$

Section S5-References

1 M. P. Gashti, J. Bellavance, O. Kroukamp, G. Wolfaardt, S. M. Taghavi, J. Greener, *Biomicrofluidics*, 2015, **9**, 041101.

2 F. Paquet-Mercier, M. P. Gashti, J. Bellavance, S. M. Taghavi, J. Greener, *Lab Chip*, 2016, **16**, 4710-4717.

3 N. Jia, A. Daignault-Bouchard, T. Deng, T. G. Mayerhöfer, A. Bégin-Drolet, J. Greener, *Lab Chip*, 2023, **23**, 3561-3570.

4 F. Asayesh, M. P. Zarabadi, N. B. Aznaveh, J. Greener, *Anal. Methods*, 2018, **10**, 4579-4587.